Structure and Aanalysis of the Eye of a Numerically Simulated Tropical Cyclone

By Yoshio Kurihara and Morris A. Bender

Geophysical Fluid Dynamics Laboratory/NOAA
Princeton University, Princeton, New Jersey 08540, U.S.A.
(Manuscript received 22 September 1981, in revised form 4 November 1981)

Abstract

A tropical cyclone has been simulated in a quadruply nested mesh model with finest grid resolution of about 5 km. At the center of the vortex, a compact eye was maintained. Azimuthal means as well as asymmetry of the eye and the eye wall structure are described. The asymmetric features within the eye wall moved cyclonically at a much smaller rotation rate than the cyclonic wind within the eye wall. Roles of the mean radial-vertical circulation, the eddy motions and the diffusion effect in the maintenance of the mean structure are analyzed. In the analysis, attention is given to the balance between the wind and pressure fields and also to the budgets of relative angular momentum, heat and water vapor. The eddy motions caused a cooling and moistening effect in the eye which counterbalanced a warming and drying effect due to the mean sinking motion.

1. Introduction

The eye is a frequently observed phenomenon in intense tropical cyclones, consisting of a relatively warm and cloud-free air column surrounded by an area of intense convection, usually called the eye wall. Asymmetric structure of the eye wall has been recognized since earlier aircraft observations (*e.g.*, Simpson, 1952; Gentry, 1963; La Seur and Hawkins, 1963).

Much effort has been made to understand certain features concerning the formation, structure and maintenance of the eye of tropical cyclones. This includes the construction of model vortices containing an eye, through analytical considerations usually combined with observational analysis (*e.g.*, Jordan, 1952; Malkus, 1958; Kuo, 1959; Eliassen, 1971; Willoughby, 1979; Smith, 1980). Composite analyses of the inner core region of observed hurricanes were made by Shea and Gray (1973) and Gray and Shea (1973). Also, laboratory experiments to simulate the eye were reported (*e.g.*, Wui and Ye, 1979). Based on the results from his axisymmetric numerical model, Ooyama (1969) discussed the effect of the non-balanced boundary layer flow on the eye structure. In Jones' (1980) three-dimensional, nested-mesh model with finest grid resolution of 10 km, an eye-like structure appeared.

One factor which remained uncertain or speculative at best in the above mentioned studies is the role of asymmetries in the dynamics of the eye. In this study, we present a fairly comprehensive and coherent picture of the eye structure including the characteristics of asymmetry. Quantitative estimates of various quantities within the eye and the eye wall were made possible by the application of a quadruply-nested movable mesh model. Although the eye we analyze is a numerically simulated one rather than an actual eye, we hope the obtained results will increase our knowledge of the eye dynamics.

In the present paper, the numerical model used and the time integration of it are briefly described in Sections 2 and 3, respectively. The time averaged, azimuthal mean of the vortex structure is shown in Section 4. In Section 5, the asymmetric features are investigated. The balance relation between the wind and pressure and the budgets of relative angular momentum, heat and water vapor are discussed in Section 6. Finally, some remarks on the present experiment are made in Section 7.

2. Brief description of the model

The numerical simulation model used in the present study is the eleven level primitive equation model constructed at the Geophysical Fluid Dynamics Laboratory, NOAA. The governing equations of the model and the computational schemes applied to it are identical to those explained in the paper by Kurihara and Bender (1980, see both text and appendices).

We used a quadruply nested grid system for making the time integration of the model. The outermost grid area defined a channel type domain, with cyclic condition assumed for its 33.2 degree longitudinal span and laterally open conditions placed at 5.2°N and 38.4°N. The grid resolution, or the meridional distance between grid points, was reduced at each nesting from 90 km to 30 km, then to 10 km, and finally to 5 km. Other information on the grid system is listed in Table 1. The inner three meshes, which were movable, were shifted during the course of the time integration so that the vortex remained in the center of these meshes.

In the present model, the hydrostatic balance is assumed and also a parameterization scheme is used to incorporate the effect of moist convection. Accordingly, an accurate simulation of transient features of individual convection elements is precluded even though the grid resolution was increased in this experiment. We presume that, when an intense vortex having the scale of a tropical cyclone evolved in the model integration, the condition of hydrostatic balance may be valid for such a vortex especially at its quasi-stationary stage. The eye structure was expected to appear as a central part of the above vortex system. We will make an evaluation on the effect of parameterization for moist convection later in Section 7.

3. Time integration of the model

The initial condition of the model was determined in a manner similar to that described by Kurihara and Bender (1980). An initial circular vortex was specified by formula (3.1) in their paper for $\sigma \geq 0.9$ and the intensity of the vortex was decreased with height above $\sigma = 0.9$ by the factor $\sigma/0.9$. (σ is the pressure normalized by its surface value.) Numerical constants in (3.1) were set as $V_m = 12 \text{ m s}^{-1}$ (maximum wind speed), $R_m = 150 \text{ km}$ (approximate radius of maximum wind) and $R_0 = 1,167 \text{ km}$ (equivalent to 10.5 degrees latitude: radial extent of vortex). The

Table   Grid system of a quadruply nested mesh model

Mesh	Grid resolution Meridional (km)	Zonal (km)	Domain size (Grid number)	Time step (sec)
1	90	90 cosϕ	41×41	126
2	30	30 cosϕ	36×36	42
3	10	10 cosϕ	36×36	14
4	5	5 cosϕ	32×32	7

ϕ: Latitude

above vortex was placed at 19.8°N. The values of the constants $T_0(\sigma)$ and p_{*0} which appear in the above mentioned paper as well as the initial relative humidity were the same values as $T(5000, \sigma)$, $p_*(5000)$ and the initial humidity, respectively, described in the paper by Kurihara and Tuleya (1974). It is important to note that no zonal flow was present at the initial time and, hence, the evolution of the vortex occurred in a calm environment.

The time integration of the model proceeded to 48 hours with the time steps listed in Table 1. During the integration, the sea surface temperature was fixed at 302K. Fig. 1 shows the time change of the radial distribution of the azimuthally averaged surface pressure. Rapid deepening of the vortex took place during the 24 to 36 hour period. A slow change in the central surface pressure after hour 36 suggests that the vortex was at a nearly stationary state in the later period. At hour 43.6, when the storm was the most intense, the minimum surface pressure and the maximum surface wind were 924 mb and 76 m s^{-1}, respectively. In the 48 hour period, the center of vortex moved 52 km to the west and 73 km to the north from the initial position, probably due to the β-effect (e.g., Adem, 1956).

At the center of the quasi-stationary vortex, a well defined area of no precipitation, which is usually an indication of the eye of a tropical
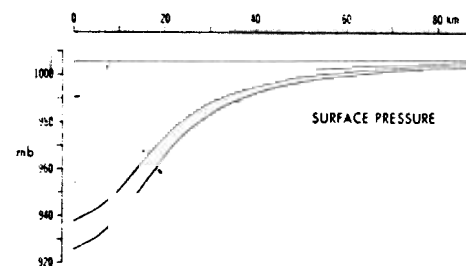

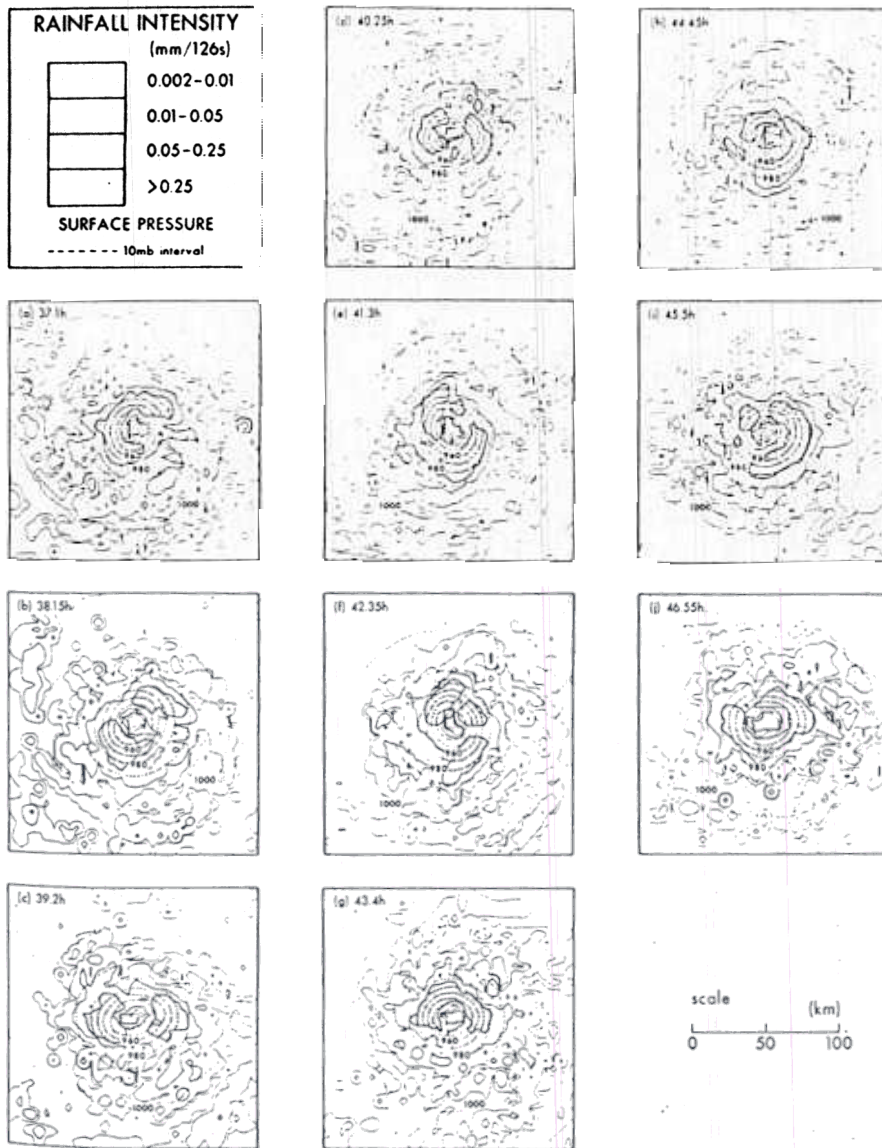Fig. 1   Radial distribution of azimuthally averaged surface pressure at 12, 24, 36 and 48 hours.

Fig. 2 ·Distribution of rainfall intensity and surface pressure at ten time levels in the period of hour 37.1 through 46.55.

cyclone, was persistently observed. (An eye-like structure was first noticed at hour 25 when the central pressure and the maximum surface wind were 983 mb and 45 m s⁻¹, respectively.) In Fig. 2, the distribution of the precipitation intensity, together with that of surface pressure at ten time levels from hour 37.1 to hour 46.55 is presented. An area of moderate and heavy rain, i.e., greater than 0.05 mm/126 s, which encircles the area of no rainfall indicates the eye wall. Apparently, the eye that developed in the present experiment was very compact. It may

be compared favorably with the eye of intense hurricanes such as Hilda of 1964, Inez of 1966 and Camille of 1969. The dark shaded area of heavy rainfall within the eye wall in Fig. 2 takes a round shape but broken at one or two openings. This suggests that there exists a few positions of maximum rainfall intensity within the eye wall. Also, it should be noted that the contours of surface pressure are elongated, though very little, toward the areas of strong rainfall. In the present case, the positions of surface pressure minimum and the eye almost coincide with each other.

4. Mean structure of the eye and the eye wall

In this section, we investigate the time averaged, axially symmetric component of various fields in the central area of the vortex. To obtain the mean fields, we first computed the azimuthal averages of quantities at various radii for each of the time levels used in Fig. 2. To compute the azimuthal average, the grid point values were interpolated onto 40 equally spaced points along each circle through bilinear interpolation. The axisymmetric fields thus obtained at the ten time levels showed little fluctuation with time. Accordingly, the mean vortex defined from the average of these fields can be considered representative of the entire analysis period. The structure of the mean vortex is shown in Figs. 3 through 6 as a function of the pressure level (ordinate) and the radial distance from the storm center (abscissa). The heavy solid lines in the figures indicate the radial distribution of the mean surface pressure.

Fig. 3 shows the height-radius distribution of the mean azimuthal wind. A vertical, dashdotted line indicates the radius of maximum azimuthal wind. It is located approximately at 20 km radius between 850 and 500 mb levels, tilts slightly outward above 500 mb and is found at about 22 km at the 200 mb level. The above mentioned nearly vertical structure is quite different from the results obtained in Jones' (1980) numerical simulation, which exhibits an excessive outslope below 500 mb. Except within the 10 km radius, the mean azimuthal wind changes sharply in the vertical in the boundary layer below the horizontal dash-dotted line in Fig. 3.

The mean radial-vertical circulation is presented in Fig. 4, in which the height-radius distribution of the mean stream function is shown. The mean stream function ϕ for the mass flux is related to the mean radial flow $\bar{u}$ and the mean vertical p-velocity $\bar{\omega}$ through the formulas $\bar{u} =$
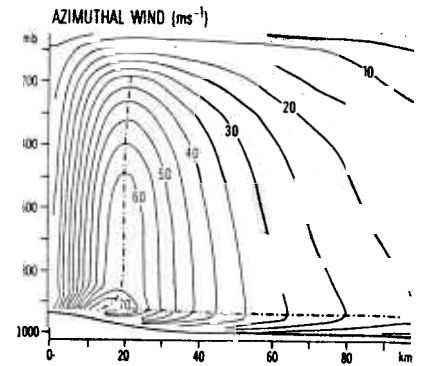

Fig. 3 Height-radius distribution, averaged for hour 37.1 through 46.55, of mean azimuthal wind (in $m\,s^{-1}$). Dash-dotted lines show the ridge lines in the distribution.
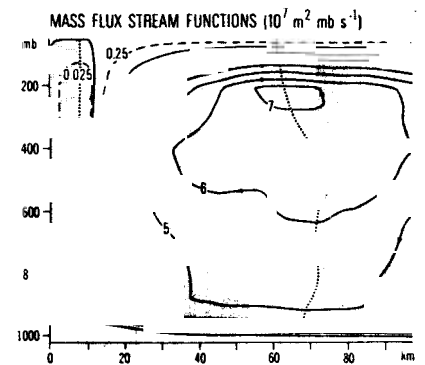

Fig. 4 Height-radius distribution, averaged for hour 37.1 through 46.55, of mean stream function, indicating the mean radial-vertical circulation (in $10^7 m^2\,mb\,s^{-1}$). The vertical velocity is zero along the dotted lines. The eye is indicated by shading.

$(1/r)\ (\partial\phi/\partial p)$ and $\omega = -(1/r)\ (\partial\phi/\partial r)$, where r and p denote the radius and the pressure, respectively. The vertical motion is zero along the dashed lines in the figure. The inner dashed line may be considered the mean inner boundary of the eye wall. The mean radius of the eye in the present case is 6.5 km up to 600 mb and gradually expands to 8 km at 200 mb. (The eye is indicated by shading in the figure.) The figure clearly shows two distinct circulation systems: one within about 10 km radius and a larger circulation system surrounding it. The inner portion, about 3.5 km wide, of the broad upward motion area at middle levels belongs to the inner circu-

lation system. The large area of upward motion is connected to the upper level outflow of the outer circulation system. The mean sinking motion within the eye is estimated to be about 0.03 mb s^{-1}. In the distribution of ω (figure not shown) an area with mean upward velocity exceeding 0.18 mb s^{-1} was observed between the 350 and 800 mb levels at around 18 km radius, *i.e.*, 2 km inside of the radius of the maximum mean azimuthal wind.

The height-radius distributions of the mean temperature anomaly, defined as the deviation from the average temperature at a corresponding level in the surrounding mesh 3 area, as well as the mean relative humidity are shown in Fig. 5 and Fig. 6, respectively. The maximum tempera-
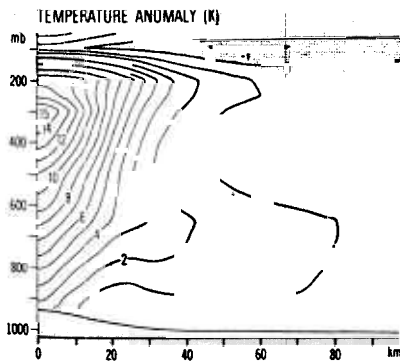

Fig. 5 Height-radius distribution, averaged for hour 37.1 through 46.55, of mean temperature departure from the average temperature of the surrounding mesh 3 area (in K). A region of negative anomaly is shaded.
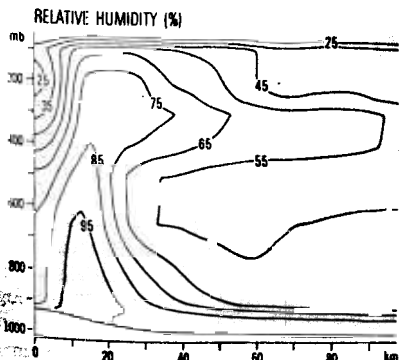

Fig. 6 Height-radius distribution, averaged for hour 37.1 through 46.55, of mean relative humidity (in per cent).
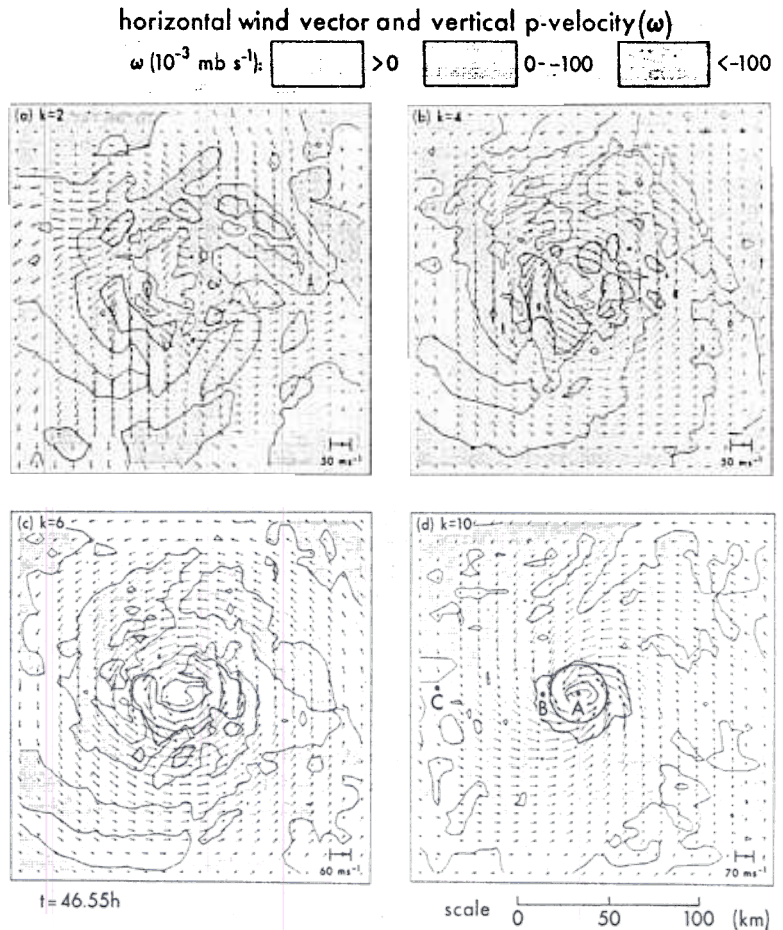
ture anomaly is 15K at the center at the 300 mb level. A weak negative anomaly exists at the 100 mb level outside the 10 km radius. According to Fig. 6, the upper half of the eye is particularly dry. A region of high mean relative humidity extends to upper levels within the eye wall. The contour for 65 per cent runs near the top of the boundary layer in the outer area, but reaches to almost the 100 mb level in the eye wall. The contour pattern suggests that the mean location of the outer boundary of the eye wall may be chosen at about 35 km radius.

5. Asymmetry of the vortex

We already noticed in Section 3 the existence of asymmetry in the structure of the eye wall. Analysis of the asymmetric or eddy component of an intense vortex is most appropriate when a zonal flow is absent as in the present case, since the definition of asymmetry becomes ambiguous in the presence of a zonal flow. As seen in Fig. 2, the asymmetric component appears to rotate within the mean vortex. Accordingly, its typical feature can more easily be depicted from the analyses of the fields at one appropriate time level. In this section, various fields at hour 46.55 are presented.

Fig. 7 shows the distributions of the horizontal wind and the vertical velocity, ω, at levels 2($\sim$15 km), 4($\sim$8.3 km), 6($\sim$3.3 km) and 10($\sim$0.2 km), respectively. The asymmetry of the horizontal wind is most evident at level 2, *i.e.*, the outflow level. The field of ω exhibits a pattern of spiral shape, especially at middle levels. While the negative (positive) ω corresponds to upward (downward) motion at the levels 2, 4 and 6, the large area of negative ω at the level 10 reflects the movement of an air parcel toward the lower pressure area. From the comparison of Fig. 7(c) and Fig. 2(j), it may be suggested that the precipitation intensity within the eye wall is correlated well with the vertical velocity at the middle levels.

The positions of the strong upward motion and, hence, the large rainfall intensity moved around the vortex center. The analysis of such movement was made. The results indicate that it takes 77 minutes on the average to make one counter-clockwise rotation. On the other hand, the rotation rate for the wind within the eye wall is, when estimated from the mean azimuthal wind of 60 m s^{-1} at the 20 km radius, 35 minutes for one rotation. Accordingly, the rotation of the asymmetry within the eye wall relative to the

horizontal wind vector and vertical p-velocity (ω)

ω (10^{-3} mb s^{-1}): [ ] >0   [ ] 0--100   [ ] <-100

t = 46.55h

scale 0   50   100 (km)

Fig. 7 Distribution of the horizontal wind vectors and vertical p-velocity at
hour 46.55, at (a) level 2 (~15 km), (b) level 4 (~8.3 km), (c) level 6
(~3.3 km) and (d) level 10 (~0.2 km). Along a circle of 17.5 km radius
and at points A, B and C, indicated in (d), analyses in Fig. 9 and 10
are made, respectively.

rotating wind is clockwise.

Asymmetry of the flow field can also be seen
in Fig. 8. In this figure, the zonal and the meri-
dional vertical cross sections through point A in
Fig. 7(d), i.e., the vortex center, are presented.
The air in the shaded area is descending. It is
seen that the upward motion is relatively strong
to the west of the vortex center and weak to the
north. The instantaneous wind at the edge of the
eye deviated significantly from the mean circu-
lation shown in Fig. 4. It will be shown later
that this asymmetric flow within the eye and the
eye wall, i.e., eddy motion, makes significant

contributions to the heat and moisture budgets.
As mentioned before, the outflow at the upper
levels is quite asymmetric.

Asymmetry within the eye wall is illustrated
in Fig. 9. This figure shows the distributions
of the vertical velocity, ω, and, the temperature
anomaly on the cross section along the circle of
17.5 km radius shown in Fig. 7(d). Roughly
speaking, the upward motion is relatively strong
south through west as well as north through east
of the center. It is fairly weak to the north-
northwest. It appears that the temperature
anomaly is negatively correlated with ω, suggest-

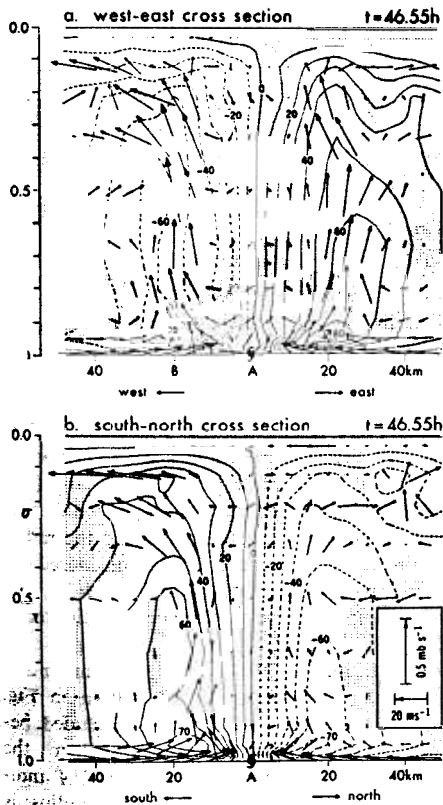RADIAL AND VERTICAL WIND (arrow)

AZIMUTHAL WIND (contour, ms⁻¹)

Fig. 8. Vertical cross sections, (a) west-east and (b) south-north, through the point A in Fig. 7(d) at hour 46.55, for the radial-vertical wind (arrow) and azimuthal wind (contour, in m s⁻¹). Areas with $\omega>0$ are shaded.

ω (——, 10^{-1} mb s⁻¹) and $T-T_0$ (- - -, K) at 17.5 km from the center   t = 46.55h

Fig. 9 Distribution of ω (solid lines, in 10^{-1} mb s⁻¹) and $T-T_0$ (dashed lines, in K. T_0 is the average temperature for the mesh 3 area) at hour 46.55, on a cylindrical surface at 17.5 km radius indicated in Fig. 7(d). Areas with $\omega>0$ are shaded.

Fig. 10 Temperature profiles at hour 46.55, at three points shown in Fig. 7(d), i.e., at A (eye), B (20 km west, eye wall) and C (75 km west). Relative humidities (in per cent) are indicated by numbers along the curves.

ing that the conversion of eddy available potential energy into eddy kinetic energy is occurring within the eye wall.

Asymmetry of the temperature anomaly as shown in Fig. 9 implies that there is significant variation of the temperature sounding within the eye wall. The temperature sounding at 20 km west of the center, i.e., at point B in Fig. 7(d), is presented in Fig. 10, together with those in the eye and the outer environment, i.e., at points A and C, respectively, in Fig. 7(d). The relative humidity is also indicated by numbers along the curves. In the eye, the air above the 300 mb level is in a nearly neutral state and quite dry.
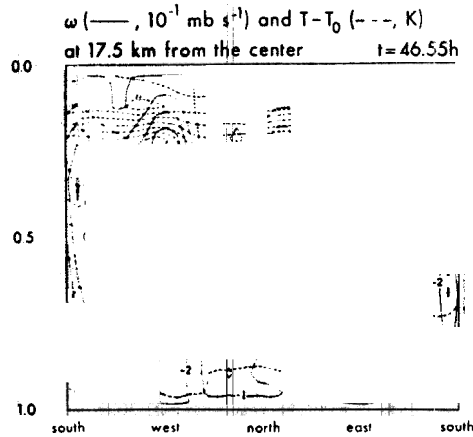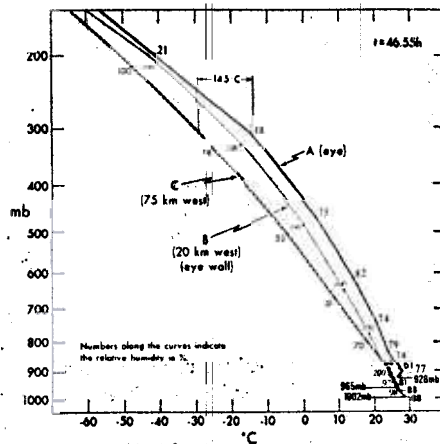
Below 300 mb, it is very stable and still far from saturation. The temperature at 300 mb is higher by as much as 14.5°C than that of the environment. The sounding curve for point B coincides with a moist adiabatic ascent. The air column at this point is saturated above the boundary layer. At point C, the air between 400 and 900 mb is relatively dry and is stable for dry

adiabatic ascent.

6. Maintenance of the mean structure of the eye and the eye wall

In this section, we investigate the role of asymmetry as well as that of mean radial-vertical circulation in the maintenance of the mean structure of the vortex. For the above purpose, we perform budget analyses of various quantities for a period during which transient features, such as the fluctuation in the distribution of vertical motion within the eye, are considered minimal. In the present time integration, such a relatively steady period is found after hour 45.435. All the results presented in this section represent the average of budgets at five time levels within a 10.5 minute period after the above time level.

In making the budget analyses, we ignore the asymmetry and the time variation of the surface pressure for simplicity. Also, since the budgets are calculated within a radius of 80 km from the storm center, we can assume that the Coriolis parameter, f, is constant; $f=5.09\times10^{-5}\,\mathrm{s}^{-1}$. The analyses are made using a cylindrical coordinate system with the σ-coordinate in the vertical. The notations used are: r (radius from storm center), u (radial wind, positive outward), v (azimuthal wind, positive counterclockwise), $\dot{\sigma}$ (vertical σ-velocity, $d\sigma/dt$), ω (vertical p-velocity, dp/dt), T (temperature), R (mixing ratio of water vapor), ϕ (geopotential of a pressure surface), p_* (surface pressure), R_g (gas constant) and c_p (specific heat of the air at the constant pressure). The overbar notation represents the azimuthal average of a quantity along a certain fixed radius. The azimuthal averages at each radius were calculated from the grid point values using the same procedure described in section 4. Deviation of a quantity from its azimuthal average is denoted by a prime. We define the operator M which expresses the advection of a quantity $\bar{x}$ by the mean circulation:

$$M(\bar{x})= -\bar{u}(\partial\bar{x}/\partial r)-\bar{\sigma}(\partial\bar{x}/\partial\sigma).$$

The operator E denotes the effect of eddy transport:

$$E(x)= -\frac{1}{\bar{p}_*}\left[\frac{\partial\bar{p}_*r\overline{u'x'}}{r\partial r}+\frac{\partial\bar{p}_*\overline{\dot{\sigma}'x'}}{\partial\sigma}\right].$$

We evaluated $\overline{u'x'}$ by $\overline{ux}-\bar{u}\bar{x}$. In obtaining $\overline{ux}$, the interpolation of grid point values onto the points along each circle was made with respect to the product ux itself. Computation of $\overline{\dot{\sigma}'x'}$ was similar.

a. Balance of forces in the radial direction

We examine a state of balance between the mean azimuthal wind and the mean pressure field. The equation for $\bar{u}$ may be written as

$$\frac{\partial\bar{u}}{\partial t}=UA+UB+UC+UD \qquad (1)$$

where

UA　imbalance from the gradient wind balance $[=(f+\bar{v}/r)\bar{v}-\partial\bar{\phi}/\partial r]$

UB　inertia effect due to the mean circulation $[=M(\bar{u})]$

UC　effect of the eddies $[=E(u)+\overline{v'v'}/r]$

UD　effect of horizontal and vertical diffusion.

The mean azimuthal wind, $\bar{v}$, is super-gradient if UA is positive, whereas it is sub-gradient if UA is negative. In the present vortex, UA is near zero everywhere except for the boundary layer and the upper level outflow layer. This means that the gradient wind is a good approximation for $\bar{v}$ at the place where $\bar{u}$ is small. (The gradient wind relation may still be valid even when $\bar{u}$ is large, if the actual wind and the radius of curvature of flow are properly considered for each air parcel. However, in this paper, we discuss the gradient wind balance only in terms of UA.)

The distributions of the budget components of (1) in the boundary layer are shown in Fig. 11. The center area ($r<7.5$ km) is excluded because of numerical difficulties related to the singularity at the center. The sign of UA indicates that $\bar{v}$ within about the 30 km radius is super-gradient except for the shallow layer outward of the 15 km radius where it is subgradient. As reflected in the distribution of $UA+UB$, the inertia effect of the mean circulation tends to cause deceleration of $\bar{u}$, leading to the reduction of the super gradient imbalance. The radial flow $\bar{u}$ becomes steady provided that $UA+UB$ is counterbalanced by the terms UC and UD. This is approximately the case as seen in Fig. 11. The role of asymmetry, i.e., UC, is not negligible particularly at the small radii.

The state of balance in the outflow layer is illustrated in Fig. 12. As shown by UA, $\bar{v}$ within about 20 km radius is subgradient and $\bar{v}$ between 20 and 40 km is supergradient. The effect of UB is to reduce the supergradient imbalance above 200 mb level. In UB, the horizontal and vertical advection of $\bar{u}$ are found to be equally important. It is clearly seen that the balance of forces at the upper levels is almost
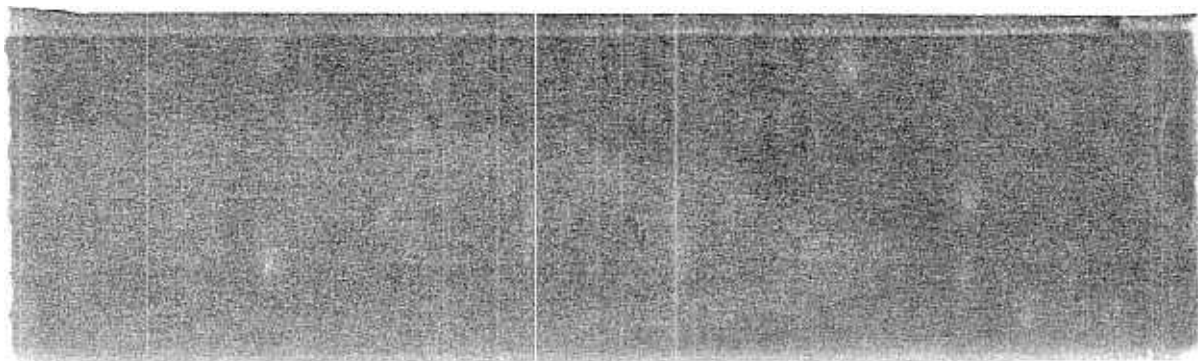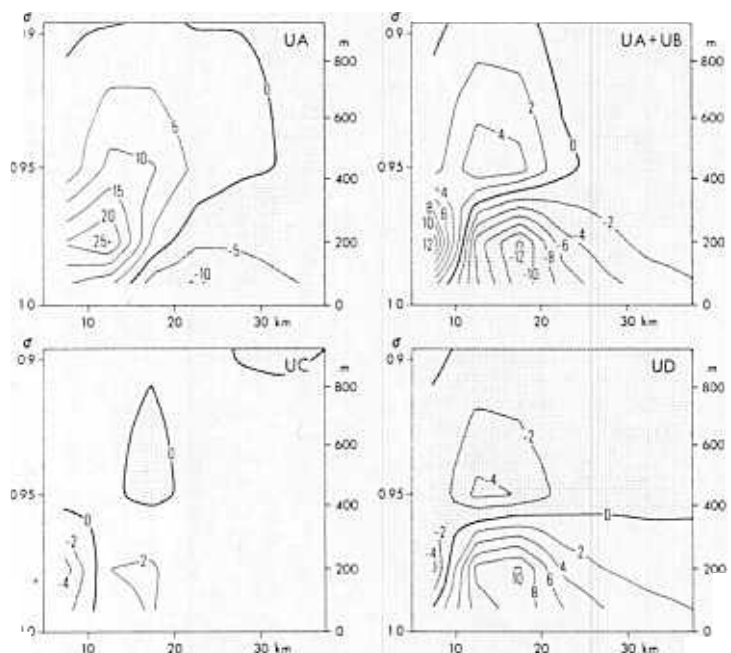
Fig. 11 Height-radius distributions of ~10 min average (at ~45.4 h)
of UA, UA+UB, UC and UD in eq. (1) for the boundary layer
(all units 10^{-2}m s^{-2}). Areas with negative values are shaded.
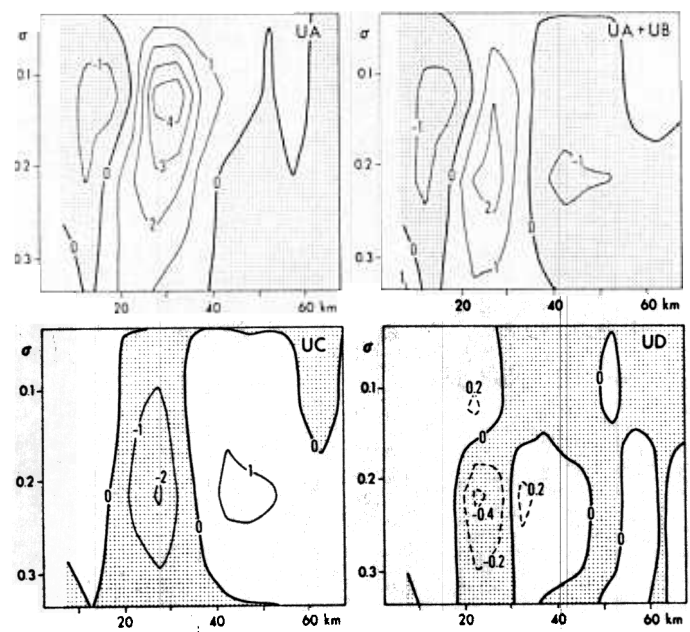

Fig. 12. As in Fig. 11 except for the outflow layer.

complete with the addition of *UC* to *UA* + *UB*. The eddy effect, *UC*, is mainly due to the horizontal eddy transport of u' at radii greater than 20 km, while it is largely due to the vertical transport at the smaller radii. The diffusion effect, *UD*, is not important at the upper levels for the steadiness of the mean circulation.

b. Budget of mean relative angular momentum

The equation for the mean relative angular momentum takes the following form,

$$\frac{\partial r\bar{v}}{\partial t} = MA + MB + MC + MD \qquad (2)$$

where:

MA   change due to the advection of absolute angular momentum by the mean radial-vertical circulation $[= M(r\bar{v}) - fr\bar{u}]$

MB   effect of eddy flux of relative angular momentum $[= E(rv)]$

MC   change due to horizontal diffusion

MD   change due to vertical diffusion.

In Fig. 13, the stream function for the mean radial-vertical circulation is superimposed on the distribution of the absolute angular momentum,

i.e., $\bar{v}r + (f/2)r^2$. If the former coincides with a contour of the latter quantity, it means that the budget of angular momentum is complete without the terms *MB*, *MC* and *MD*. Otherwise, these terms play a role in the maintenance of the
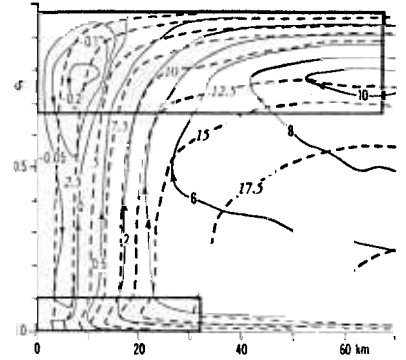

Fig. 13   Height-radius distribution of $\sim$10 min average (at $\sim$45.4 h) of mean absolute angular momentum (dashed lines, in $10^5 m^2 s^{-1}$) and mean stream function (solid lines, in $10^7 m^2$ mb s^{-1}). The boxes show the domains for which Figs. 14 and 15 are prepared, respectively.

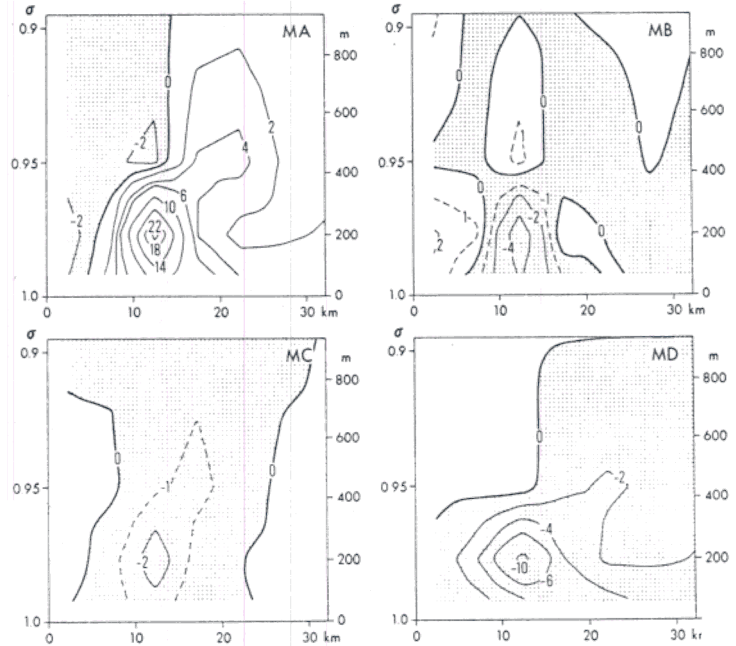Fig. 14   Height-radius distribution of $\sim$10 min average (at $\sim$45.4 h) of the budget components of relative angular momentum, *i.e.*, the terms in eq. (2), for the boundary layer (all units $10^2 m^2 s^{-2}$). Areas with negative values are shaded.

relative angular momentum of the mean vortex. In the present case, an appropriate contribution of MB, MC and MD is required at the two domains indicated in Fig. 13.

The distributions of the budget components in the boundary layer are shown in Fig. 14. The mean inflow brings larger momentum into the bottom part of the eye wall area, whereas the outward advection within the eye causes the decrease of momentum. In general, the vertical advection tends to reduce the above changes due to the horizontal advection. The resultant effect is found in the distribution of MA. It is evident from the figure that an apparent sink of momentum within the eye, negative MA, is mostly compensated by the momentum supply due to eddies, MB. The apparent source in the eye wall region, positive MA, is balanced by MD and, to a lesser but significant degree, by MB and MC. Thus, the angular momentum field of the mean vortex is kept steady.

The budget of relative angular momentum in the outflow layer is illustrated in Fig. 15. In this layer, the vertical advection of the angular momentum causes the apparent source within the eye wall. The apparent sink at the large radii results from the horizontal advection. Such advection effects of the mean radial-vertical circulation, MA, are almost entirely counter-balanced by the effect of eddies, MB. The contributions of MC and MD are small by an order of magnitude.

c. Heat budget

The equation for the mean temperature is written as

$$\frac{\partial \bar{T}}{\partial t} = TA + TB + TC + TD \qquad (3)$$

where:

TA change due to the mean radial-vertical circulation $[=M(\bar{T})+(R_g/c_p)\,(\bar{T}\bar{\omega}/p)]$

TB change due to eddy motion $[=E(T)+(R_g/c_p)\,(\overline{T'\omega'}/p)]$

TC change due to horizontal and vertical diffusion

TD change due to condensation-convection.

The distribution of potential temperature of the mean vortex, together with that of the mean stream function, is shown in Fig. 16. Since the air is stably stratified as seen in the figure, the mean sinking motion in the eye and the mean ascending motion within the eye wall causes warming and cooling, respectively. This effect, represented by TA, has to be nullified by $TB + TC + TD$ in order to maintain the stability of the mean vortex.
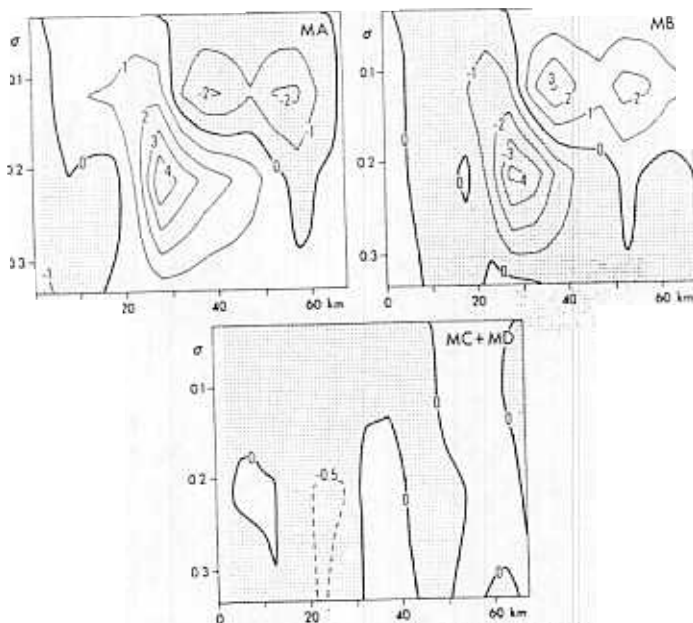

Fig. 15   As in Fig. 14 except for the outflow layer

The analysis results of the heat budget for the domain indicated in Fig. 16 are presented in Fig. 17. The above mentioned effect of the mean circulation is reflected in the distribution of TA. The role of eddies, TB, is to remove the heat from the eye at all levels to enable a nearly

Fig. 16   Height-radius distribution of ∼10 min average (at ∼45.4 h) of mean potential temperature (dashed lines, in K) and mean stream function (solid lines, in $10^7 m^2 mb s^{-1}$). The box shows the domain for which Figs. 17 and 18 are respectively prepared.

stationary state in the eye to be maintained. It is found that the horizontal eddy flux is a major contributing factor in TB. The role of TB is also seen in the outflow layer. The diffusion TC serves mainly to supply heat into the boundary layer. The apparent heat sink, i.e., the negative TA, within the eye wall is compensated to a large degree by the diabatic heating effect, TD. The quantity TD is related to the conversion of latent energy into total potential energy. In the present model, such a conversion integrated within the 67.5 km radius is 2.415×10^{14} W. On the other hand, the conversion of total potential energy into mean kinetic energy, which is expressed by $-\bar{u}\, \partial\bar{\phi}/\partial r$, integrated for the same domain is 13.51×10^{12} W, and the conversion into eddy kinetic energy, $-v' \cdot \nabla \phi'$ (v and ∇ are the horizontal wind and the gradient operator, respectively), is only 0.63×10^{12} W. Accordingly, the heat engine efficiency in the inner region of the present vortex, which is given by the ratio of the conversion of potential to kinetic energy against the conversion from latent to potential energy, is approximately 6%.
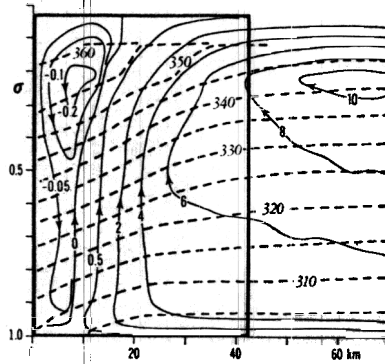
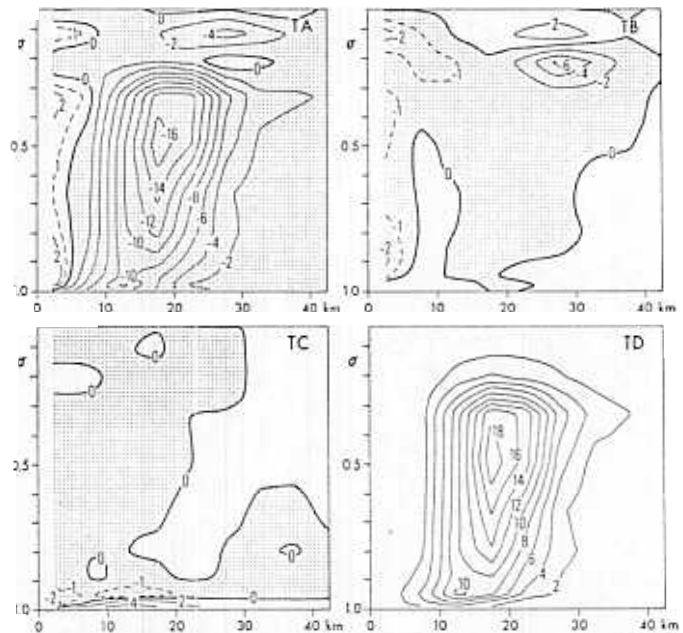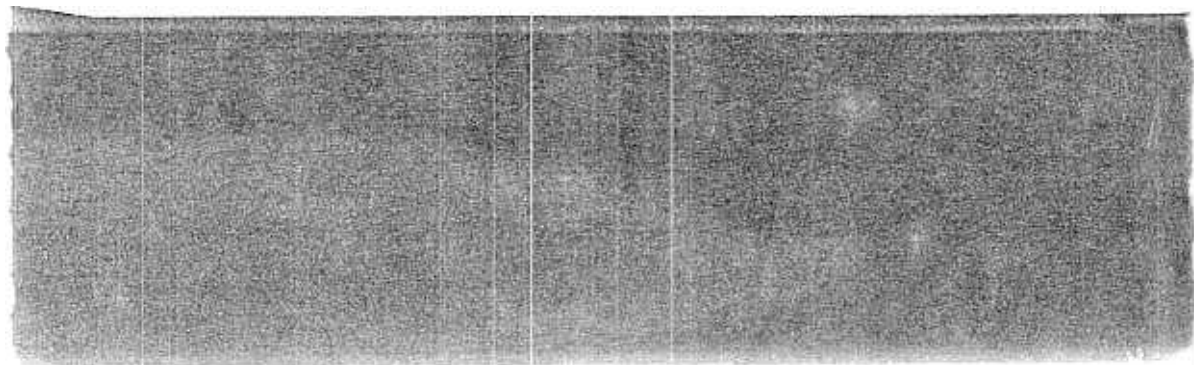d. Budget of water vapor

The budget of the mean mixing ratio of the

Fig. 17   Height-radius distribution of ∼10 min average (at ∼45.4 h) of the heat budget components, i.e., the terms in eq. (3), (all units $10^{-3} K s^{-1}$). Areas with negative values are shaded.

water vapor is analyzed using the following equation,

$$\frac{\partial R}{\partial t} = RA + RB + RC + RD \qquad (4)$$

where:

RA change due to the mean radial-vertical circulation $[=M(R)]$
RB change due to the eddy motion $[=E(R)]$
RC change due to horizontal and vertical diffusion
RD change due to condensation-convection.

The distributions of each term in the above equation are shown in Fig. 18. The mean sinking in the eye has a drying effect, resulting in the negative RA, while the upward motion within the eye wall causes moistening, i.e., positive RA. The above mentioned drying effect in the eye is largely offset by the moisture supply by the eddies, RB. Horizontal mixing by eddies is found to be a predominant factor in RB. The diffusion effect, RC, serves to increase the mixing ratio in the boundary layer including that region contained within the eye. The effect of condensation, RD, balances the positive RA within the eye wall.

7. Summary and remarks

Using a quadruply nested mesh model with a finest grid resolution of about 5 km, a quasi-stationary tropical cyclone is simulated. At the center of the vortex, a compact eye is maintained. The radius of the eye is about 6.5 km below 600 mb and increases to 8 km at 200 mb. Within the eye, a weak mean sinking motion exists, free from rainfall. The temperature anomaly of the eye is 15 K at 300 mb. Note that the above vortex is maintained in a calm environment. One of the problems to be studied in the future is to find the factors which determine the size and intensity of a quasi-stationary vortex. In this respect, it may be informative to mention that Kurihara and Tuleya (1974), using a model similar to the present one except for the horizontal resolution and the treatment of vertical mixing, obtained a larger vortex than the present one in an integration which started from an initial vortex with a much larger radial extent. On the other hand, the vortex which evolved from the initially rest state in a high resolution, axisymmetric, deep convection model (Yamasaki, 1977) was much smaller than the
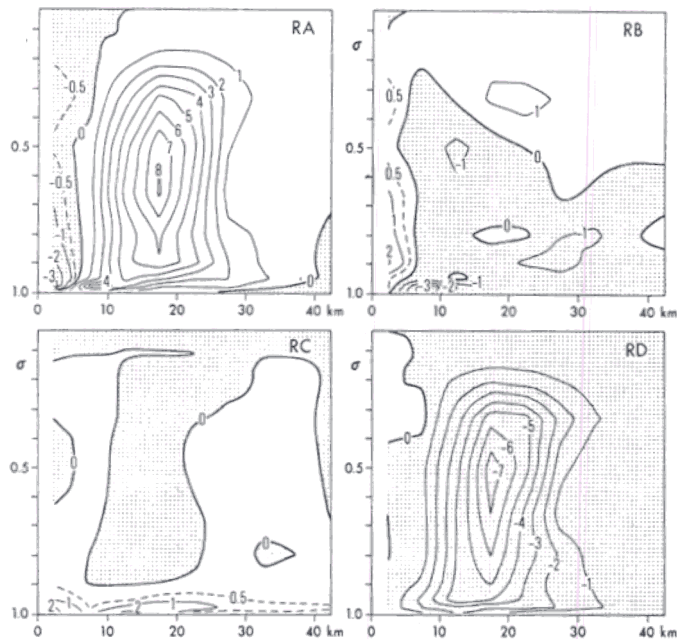

Fig. 18 Height-radius distribution of ~10 min average (at ~45.4 h) of the water vapor budget components, i.e., the terms in eq. (4), (all units 10^{-3} g kg^{-1} s^{-1}). Areas with negative values are shaded.

present one. We speculate that relatively weak winds beyond a certain radius, either due to lack of basic flow or small size of vortex, will reduce the evaporation rate and, hence, may weaken the convective activity in the outer domain.

Asymmetry in the vortex structure is evident in various fields. Areas of anomalous rainfall intensity and ascending motion are observed at a few locations within the eye wall. The asymmetric features within the eye wall move cyclonically with a much smaller rotation rate than the wind within the eye wall.

Except for the boundary layer and the upper outflow layer, the mean vortex is in gradient wind balance. In the above two layers, a state of balance is achieved with the inclusion of the inertia effect of the mean radial-vertical circulation, the stress effect of the eddy motions and the effect of diffusion. The frictional effect is also important in the boundary layer. If a basic flow is present, the balance of forces within the vortex is affected. According to the analysis by La Seur and Hawkins (1963), the radius of curvature of the flow will vary around the storm in this case, although the gradient wind is still a good approximation to the actual wind in the free atmosphere.

In the budget of relative angular momentum, the effect of the mean circulation is offset by either or both of the effects due to eddies and diffusion. The eddies supply angular momentum to the bottom part of the eye and remove angular momentum from the surrounding boundary layer.

The warming and drying in the eye due to mean sinking motion are counterbalanced by the cooling and moistening effect of the eddies. This effect is apparently caused at each level by the exchange of the air between the warm, dry eye and the relatively cool, moist eye wall. It should be noted here that the heat and moisture budgets presented in this paper are obtained from a rather simple model. The analysis results may have to be modified if the effects which are absent in the present model, such as the evaporation of falling raindrops and the suspension of cloud droplets, play significant roles in the budget.

The budget analyses in the present study were made for a particular ten minute period. The eddies represent the deviation from the axisymmetric field at each of the time levels. The local sum of the budget components for certain quantities at one arbitrary time level is not necessarily small, indicating fluctuation of the mean fields. We note here that the axisymmetric fields

in the previously mentioned Yamasaki's model (1977) exhibited short period oscillation as well as small scale radial-vertical variation.

As mentioned in Section 2, a parameterization scheme for the moist convection (Kurihara, 1973) is incorporated in the present model. In order to examine the degree of impact of the parameterization on the structure of a mature vortex, a supplemental integration was performed. In this case, the parameterization scheme was removed from the model at hour 37.1, after the eye was established, and the integration was continued for about an 8.5 hour period. The vortex structures from the two models, with and without the parameterization effect, were then compared with each other. It was found that the overall structures are about the same. This suggests that, in case of the grid resolution of 5 km, a large part of the heat and moisture fields within the eye wall area at the mature stage of the storm are determined by the explicit motion and that the contribution of the sub-grid scale convection is rather small. (Convection in the outer area in the two integrations was too weak to make a definite evaluation of the parameterization effect.) It also appears that the asymmetric features may be strongly dependent on the mean vortex structure, rather than the sub-grid scale convection. The ground for this conjecture is that the patterns of asymmetry in two numerical models, namely the present model and the model by Kitade (1980), are quite similar to each other in various respects despite the use of different parameterization schemes.

References

Adem, J., 1956: A series solution for the barotropic vorticity equation and its application in the study of atmospheric vortices. *Tellus*, 8, 364-372.

Eliassen, A., 1971: On the Ekman layer in a

circular vortex. *J. Meteor. Soc. Japan*, **49**, 784-789.

Gentry, R. C., 1963: Structure of tropical storms. Proceedings of the inter-regional seminar on tropical cyclones in Tokyo, 18-31 Jan. 1962, Japan Meteorological Agency, 133-158.

Gray, W. M., and D. J. Shea, 1973: The hurricanes inner core region. II. Dynamic and thermodynamic characteristics. *J. Atmos. Sci.*, **30**, 1565-1576.

Jones, R. W., 1980: A three-dimensional tropical cyclone model with release of latent heat by the resolvable scales. *J. Atmos. Sci.*, **37**, 930-938.

Jordan, C. L., 1952: On the low-level structure of the typhoon eye. *J. Meteor.*, **9**, 285-290.

Kitade, T., 1980: Numerical experiments of tropical cyclones on a plane with variable Coriolis parameter. *J. Meteor. Soc. Japan*, **58**, 471-488.

Kuo, H. L., 1959: Dynamics of convective vortices and eye formation. *The Atmosphere and Sea in Motion*, Rossby Memorial Volume, B. Bolin, Ed., Rockefeller Institute Press, 413-424.

Kurihara, Y., 1973: A scheme of moist convective adjustment. *Mon. Wea. Rev.*, **101**, 547-553.

————, and R. E. Tuleya, 1974: Structure of a tropical cyclone developed in a three-dimensional numerical simulation model. *J. Atmos. Sci.*, **31**, 893-919.

————, and M. A. Bender, 1980: Use of a movable nested-mesh model for tracking a small vortex. *Mon. Wea. Rev.*, **108**, 1792-1809.

La Seur, N. E., and H. F. Hawkins, 1963: An analysis of Hurricane Cleo (1958) based on data from research reconnaissance aircraft. *Mon. Wea. Rev.*, **91**, 694-709.

Malkus, J. S., 1958: On the structure and maintenance of the mature hurricane eye. *J. Meteor.*, **15**, 337-349.

Ooyama, K., 1969: Numerical simulation of tropical cyclones with an axisymmetric model. Proceedings of the WMO/IUGG Symposium on numerical weather prediction in Tokyo, Nov. 26-Dec. 4, 1968. Japan Meteorological Agency. III 81-88.

Shea, D. J., and W. M. Gray, 1973: The hurricanes inner core region. I Symmetric and asymmetric structure. *J. Atmos. Sci.*, **30**, 1544-1564.

Simpson, R. H., 1952: Exploring eye of typhoon 'Marge', 1951. *Bull. Amer. Met. Soc.*, **33**, 286-298.

Smith, R. K., 1980: Tropical cyclone eye dynamics. *J. Atmos. Sci.*, **37**, 1227-1232.

Willoughby, H. E., 1979: Forced secondary circulations in hurricanes. *J. Geophys. Res.*, **84**, 3173-3183.

Wui, Ding-wen and Du-Zheng Ye, 1979: The structure and the formation of spiral bands of the tropical storms—an experimental simulation. *Acta Meteorologica Sinica*, **37**, 16-28.

Yamasaki, M., 1977: A preliminary experiment of the tropical cyclone without parameterizing the effects of cumulus convection. *J. Meteor. Soc. Japan*, **55**, 11-31.

数値的にシミュレートした熱帯低気圧の眼の構造と解析

栗原宜夫・Morris A. Bender

Geophysical Fluid Dynamics Laboratory, NOAA, U.S.A.

最小格子間隔約5kmの4重格子数値モデルを用いて，熱帯低気圧のシミュレーションを行なった。得られた渦の中心には小さな眼が維持された。

眼と眼の壁の構造に関し，軸対称の場と非対称性について記述する。眼の壁の非対称の場は眼の回りを低気圧性に動くが，その回転速度は，眼の壁の中の風よりもかなりおそいことが分かった。また平均場を維持する上で，平均鉛直面循環，擾乱，および拡散効果が果たす役割を解析する。その場合，特に，風と気圧場の釣合の問題と，相対角運動量，熱および水蒸気の収支に注目する。擾乱の場は，眼の内部に冷却・湿潤効果をもたらし，これが，平均下降流による温暖・乾燥効果を相殺していることが判明した。